Clipped random wave analysis of isometric lamellar microemulsions

Dawen Choy[1] and Sow-Hsin Chen[2,*]
[1]*Department of Physics, Massachusetts Institute of Technology, Cambridge, Massachusetts 02139*
[2]*Department of Nuclear Engineering, Massachusetts Institute of Technology, Cambridge, Massachusetts 02139*
(Received 5 August 1999)

We have made small angle neutron scattering studies of $C_{10}E_4$-D_2O-octane isometric microemulsions in the lamellar phase at the hydrophile-lipophile balance temperature. The scattering intensity distributions were then analyzed with a particular choice of a spectral density function (SDF) derived by maximization of generalized entropy. The model agrees well with the measured intensities on an absolute scale, and allowed us to derive various length scales associated with the microemulsion mesoscopic structure as well as the average interfacial curvatures. We also used the experimentally determined SDF to generate a three-dimensional snapshot of the fluctuating microemulsion microstructure. Unlike conventional pictures of extended lamellar planes, we observed small domains which were internally lamellar but randomly oriented with respect to each other. Finally, we computed the probability distributions of the mean curvature H and the Gaussian curvature K on the oil-water interface. The former showed a symmetric distribution centered around $H = 0$, while the latter showed a skewed distribution peaked at a negative value of K, but with a wing extending to positive values.

PACS number(s): 82.70.−y

I. INTRODUCTION

Microemulsions are amphiphilic solutions containing oil, water and surfactant which appear macroscopically miscible but in reality are phase separated on a microscopic scale, with the oil and water domains held in contact by the surfactant molecules. Depending on external parameters such as temperature and the relative volume ratios of oil, water, and surfactant, they exhibit a rich variety of internal structures including globular micelles, disordered bicontinuous membranes, and stacked lamellar planes.

In recent years, techniques such as light, x-ray, or neutron scattering have yielded a wealth of information about these different structures. In particular, the L_α lamellar phase has attracted a lot of interest because it is fairly common in amphiphilic systems and is easily characterized by its rotation of polarized light. Since the L_α phase consists of alternating sheetlike domains of water and oil stacked at regular intervals, a Bragg peak is typically observed in the scattering pattern, corresponding to the repeating distance of the lamellar planes [1,2].

At moderate concentrations of surfactant where the repeating distance is greater than the range of ordinary molecular interactions between neighboring lamellar sheets, the persistence of the L_α phase is usually explained by an effective steric repulsion between the sheets resulting from the constraint of nonintersection. This constraint lowers the configuration entropy and therefore raises the free energy, leading to an effective repulsive force between lamellar sheets that maintains the smectic order. Per unit area, the free energy change has the form [3]

$$\Delta F/A \propto 1/d^2, \tag{1}$$

where d is the lamellar repeating distance. Consequently, if d is large, the repulsive force is weak and thermal fluctuations in the oil-water interface may become significant enough to disrupt the smectic order. For amphiphilic membranes, which are characterized by low interfacial tension and a small bending constant, thermal fluctuations are even more important and can give rise to many topological defects in the lamellar structure, such as intermembrane passages. It has further been shown theoretically that these passages induce entropic attractive interactions that compete with the Helfrich steric repulsion, thus promoting the collapse of the regular lamellar structure when fluctuations are strong enough [4].

When the formation of passages between membranes become common, a disordered lamellar phase characterized by short range positional order may result [5]. To investigate this possibility, we conducted neutron scattering experiments on a series of $C_{10}E_4$-D_2O-octane lamellar microemulsions where the surfactant volume ratios were fairly low so that d would be on the order of 10^2 Å if a stacked structure were formed. The clipped random wave model was then used to analyze the scattering data in order to generate a real-space picture of the microemulsion as well as derive the probability distributions of the Gaussian and mean curvatures on the oil-water interface. From our results, it was clear that at high dilutions the regular lamellar structure broke down due to the proliferation of topological defects induced by thermal fluctuations.

II. CLIPPED RANDOM WAVE MODEL

Small angle neutron scattering has traditionally been used as a noninvasive technique for probing the length scales and the specific interfacial area of disordered bicontinuous microemulsions on a scale of several hundred angstroms [6]. In recent years, through the use of the clipped random wave model (CRW) [7], it has become possible to analyze the scattering intensity distribution of these microemulsions to obtain, in addition, various average interfacial curvatures and

*Electronic address: sowhsin@mit.edu

their interfacial morphologies [8]. In this paper, we shall use the CRW model with a spectral density function (SDF) chosen according to the principle of maximum entropy to analyze the scattering profiles of the dilute lamellar microemulsions.

In the CRW model [7], the order parameter field of a microemulsion system is first expanded in a series of spherically symmetric cosine waves with the magnitude of wave vectors $\mathbf{k}_n$ (isotropically distributed) chosen from a distribution function $f(k)$, and with random phases ϕ_n uniformly distributed within the interval $[0,2\pi)$

$$\psi(\mathbf{r}) = \sqrt{\frac{2}{N}} \sum_{1}^{N} \cos(\mathbf{k}_n \cdot \mathbf{r} + \phi_n). \tag{2}$$

The order parameter field is normalized in such a way that $\langle |\psi|^2 \rangle = 1$. The oil-water interface is then generated by clipping the order parameter at a level α determined by the relative volume fractions of each component, resulting in an oil-water interface that is mathematically defined as

$$\psi(\mathbf{r}) = \alpha. \tag{3}$$

For the purpose of calculating the Debye correlation function [9] in a bulk contrast experiment, the clipping operation generates a two-level field $\zeta(\mathbf{r})$ from the original, continuous field $\psi(\mathbf{r})$ by assigning $\zeta(\mathbf{r}) = 1$ (oil region) when $\psi(\mathbf{r}) \geqslant \alpha$, and $\zeta(\mathbf{r}) = 0$ (water region) when $\psi(\mathbf{r}) < \alpha$. Then the Debye correlation function is the normalized form of the two-point correlation function $\langle \zeta(\mathbf{0}) \zeta(\mathbf{r}) \rangle$. For an isometric microemulsion, where the volume fractions of the oil and water regions are equal, $\alpha = 0$. In order to treat the three-component microemulsion as an effective two-component system, we partition half (tail) of the surfactant into the oil region and the other half (head) into the water region. The scattering intensity and various geometrical quantities associated with the surface defined by Eq. (3) can then be calculated using the spectral function $f(k)$. First, by taking its Fourier transform, the two-point correlation function $g(|\mathbf{r}_1 - \mathbf{r}_2|) = \langle \psi(\mathbf{r}_1) \psi(\mathbf{r}_2) \rangle$ is obtained,

$$g(r) = \int_0^\infty \frac{\sin(kr)}{kr} \, 4\pi k^2 f(k) dk. \tag{4}$$

The Debye correlation function for isometric microemulsions can then be calculated from $g(r)$,

$$\Gamma(r) = \frac{2}{\pi} \sin^{-1}[g(r)], \tag{5}$$

from which the theoretical scattering intensity is derived as [9]

$$I(Q) = \langle \eta^2 \rangle \int \frac{\sin(Qr)}{Qr} \, 4\pi r^2 \Gamma(r) \, dr, \tag{6}$$

where $\langle \eta^2 \rangle = (\Delta\rho)^2 \varphi_1 \varphi_2$, $\Delta\rho$ being the difference between the scattering length densities of component 1 and 2 (contrast), and φ_1, φ_2 being their respective volume fractions.

The CRW model also allows us to calculate the average Gaussian and mean square curvatures of the oil-water interface from the moments of the spectral function $f(k)$ and the clipping level [10]. In particular, the total interfacial area per unit volume is proportional to the square root of the second moment $\langle k^2 \rangle$. For an isometric microemulsion where $\alpha = 0$, the average mean curvature is always $\langle H \rangle = 0$ and

$$\langle K \rangle = -\frac{1}{6} \langle k^2 \rangle, \tag{7a}$$

$$\langle H^2 \rangle = \frac{1}{6} \langle k^2 \rangle \left(\frac{6}{5} \frac{\langle k^4 \rangle}{\langle k^2 \rangle^2} - 1 \right). \tag{7b}$$

III. THEORY FOR SDF

Previous studies of bicontinuous microemulsions have used inverse polynomial forms of $f(k)$ [8] consistent with the Gaussian approximation within the Landau-Ginzburg framework. Although these spectral functions have produced good fits to experimental data, there has not been sufficient theoretical justification for their functional forms. In this paper, we shall use entropy considerations to derive a functional form of $f(k)$.

We begin by considering the expression for generalized entropy associated with the probability distribution function $f(k)$ [11],

$$\frac{S_q}{k_B} = \frac{1 - \int f^q(k) d^3k}{q - 1} \tag{8}$$

which, in the limit of $q \to 1$, reduces to the familiar Boltzmann expression

$$S = -k_B \int f(k) \ln f(k) d^3k. \tag{9}$$

We require that $f(k)$ be normalizable and that its generalized second and fourth moments exist, so as to preserve the Legendre-transformation structure of thermodynamics [11] and also produce a nonzero peak in the SDF. Following the method of Tsallis [12], these constraints can be expressed as

$$1 = \int f(k) d^3k,$$

$$\langle k^2 \rangle_q = \int k^2 f^q(k) d^3k, \tag{10}$$

$$\langle k^4 \rangle_q = \int k^4 f^q(k) d^3k.$$

Maximizing the entropy subject to these constraints, we obtain an expression for the functional form of $f(k)$,

$$f(k) = \left[\frac{-\left(\lambda + \frac{1}{q-1} \right)}{\frac{-q}{q-1} + \mu q k^2 + \nu q k^4} \right]^{1/(q-1)}, \tag{11}$$

where λ, μ, and ν are the Lagrange multipliers for each of the constraints.

$1/(q-1)$ is restricted to positive integer values, since negative indices would produce an unnormalizable spectral function, and noninteger indices would result in fractional powers of k, which is inconsistent with a Landau-Ginzburg description of the system. Also, for the ordinary second and fourth moments to exist, the spectral function must be of at least inverse eighth order, hence $1/(q-1)$ has to be greater than 1.

The values of q are thus restricted to 1,3/2,4/3, and so on. For this study, we ignored the higher order functional forms and chose $q=1$ and $q=3/2$, thereby generating an exponential form and an inverse eighth order polynomial form

$$f_1(k)=\exp(\lambda+\mu k^2+\nu k^4),$$

$$f_{3/2}(k)=\frac{4(\lambda+2)^2}{9(\nu k^4+\mu k^2-2)^2}. \tag{12}$$

For mathematical simplicity, we dropped the k^4 term in the exponential to reduce $f_1(k)$ to Gaussian form. This is equivalent to dropping the constraint of the fourth moment in Eq. (10), which is unnecessary since the Gaussian exponential possesses all even-order moments anyway. Furthermore, it can be observed that $f_{3/2}(k)$ is the square of an inverse fourth order polynomial. For microemulsions, the normalized Teubner-Strey spectral function

$$f_{\mathrm{TS}}(k)=\frac{b/\pi^2}{k^4-2(a^2-b^2)k^2+(a^2+b^2)^2} \tag{13}$$

is a useful functional form that relates the domain size $d=2\pi/a$ and the correlation length $\xi=1/b$ to the two parameters a and b in the spectral function. Since the two Lagrange multipliers μ and ν can be recast into the two parameters a and b without loss of generality, we therefore choose $f_{3/2}\sim(f_{\mathrm{TS}})^2$, resulting in the normalized spectral functions

$$f_1(k)=\frac{1}{(2\pi\sigma_k^2)^{3/2}}\exp\left(-\frac{k^2}{2\sigma_k^2}\right),$$

$$f_{3/2}(k)=\frac{8}{\pi^2}\frac{b^3(a^2+b^2)}{[k^4-2(a^2-b^2)k^2+(a^2+b^2)^2]^2}. \tag{14}$$

The final spectral function is then taken to be a linear superposition of the two forms

$$f(k)=\beta f_1(k)+(1-\beta)f_{3/2}(k). \tag{15}$$

With this form of the spectral function, the two-point correlation functions can be expressed as

$$g_1(r)=\exp\left(-\frac{\sigma_k^2 r^2}{2}\right),$$

$$g_{3/2}(r)=\frac{\exp(-br)}{a^3 r}[(a^2+b^2+a^2br)\sin(ar) - ab^2r\cos(ar)], \tag{16}$$

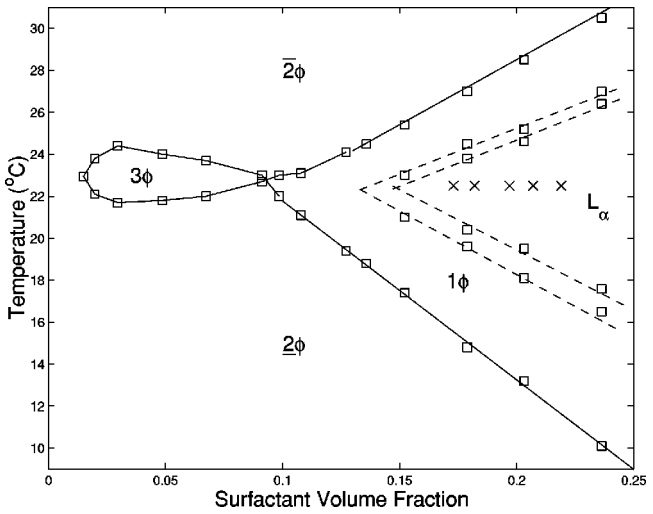

FIG. 1. Phase diagram of the $C_{10}E_4$-octane-D_2O system.

while the ordinary second and fourth moments are calculated to be

$$\langle k^2\rangle=3\beta\sigma_k^2+(1-\beta)(a^2+b^2),$$

$$\langle k^4\rangle=15\beta\sigma_k^4+(1-\beta)(a^2+b^2)(a^2+5b^2). \tag{17}$$

IV. EXPERIMENTS

The validity of our proposed spectral function was then tested by using it to analyze the scattering patterns of $C_{10}E_4$-octane-D_2O microemulsions in the lamellar phase. The scattering experiments were conducted using time-of-flight spectroscopy on the SAND instrument at the Intense Pulsed Neutron Source, Argonne National Laboratories. The surfactant volume fraction of the samples was varied from 17.3 to 21.9 % and they were all maintained at a temperature of 22.5 °C, as shown in the phase diagram above.

Proper analysis of the sharp scattering peak of lamellar systems required Q-resolution correction, and this was accomplished by convolving the theoretical scattering intensity with a Gaussian resolution function. Values for the Q width of the resolution function were supplied by Thiyagarajan [13]. After subtracting the background due to incoherent scattering, relatively good fits were obtained by analyzing the data with the spectral function in Eqs. (14) and (15), as shown in Figs. 1 and 2. From the inset, which compares the scattering intensities of bicontinuous (13.2%) and lamellar (21.9%) microemulsions, it is also clear that lamellar systems have a much sharper scattering peak.

Looking carefully at the scattering pattern, however, there were already clues that our highly dilute lamellar microemulsions did not possess the usual stacked structure of L_α microemulsions. The 2D scattering pattern was isotropic, which is not expected for the L_α phase, and the radially averaged 1D scattering peak was rather broad, even after correcting for resolution (see Fig. 3). This meant that our samples did not possess a regular layered structure, otherwise a Bragg peak would have been observed.

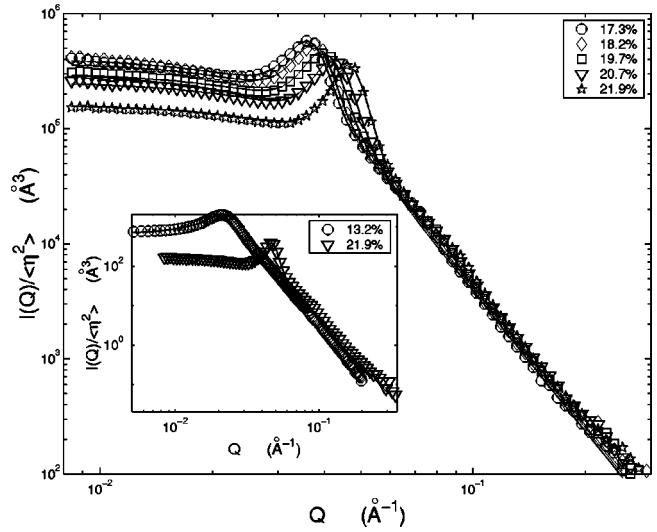

FIG. 2. Scattering intensities of lamellar samples and their fits (solid lines). In the inset, we compare the scattering intensities of bicontinuous (13.2%) and lamellar (21.9%) samples.

V. RESULTS AND DISCUSSION

Figure 4 summarizes the variation of the fitted parameters as a function of surfactant volume fraction, and clear trends can be observed from the plots. The degree of local order can be expressed as the ratio of the correlation length to the domain size, ξ/d, which is equivalent to $a/2\pi b$. The first graph in Fig. 4 thus shows that local order increases as the surfactant volume fraction φ_s is raised, which is consistent with the fact that the steric interaction between neighboring surfaces increases as the domain size decreases.

The increasing order of the microemulsion system as a function of φ_s is also reflected in the increase in σ_k and the decrease in β. A spectral function centered around $k=0$ is characteristic of disordered scattering due to the dominant contribution from long wavelength fluctuations. The falling values of β, which describes the relative contribution of the zero-mean Gaussian $f_1(k)$ to the overall spectral function in Eq. (15), is thus expected as the system gains local order. At the same time, the increasing values of σ_k reflects the decreasing importance of long wavelength contributions to the overall scattering intensity.

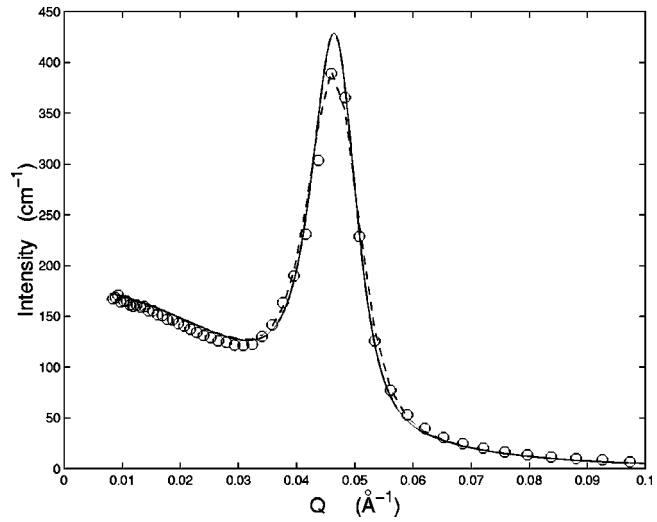

FIG. 3. Theoretical scattering intensity of a lamellar microemulsion ($\varphi=21.9\%$) before resolution correction (solid line) and after correction (dashed line).

Figure 4 also shows that the mean Gaussian curvature $\langle K\rangle$ becomes more negative with φ_s, while the mean square curvature $\langle H^2\rangle$ increases. The declining value of $\langle K\rangle$ is likely due to the increasing number of topological defects in the lamellar surfaces as more and more surfactant molecules are packed into the surfaces. The tighter packing also results in a slight increase in surface fluctuations, which accounts for the rising values of $\langle H^2\rangle$. However, compared to previously measured values of $\langle H^2\rangle$ for bicontinuous microemulsions [8], these values are smaller by almost a factor of 5, indicating the relative smoothness of the interface.

We also found an empirical linear relationship between the domain size $2\pi/a$ and the inverse of the surface-volume ratio, as shown in Fig. 4. This relationship can be used together with the equation

$$\frac{S}{V}=\frac{2}{\pi}\sqrt{\frac{\langle k^2\rangle}{3}}, \tag{18}$$

to eliminate one of the four fitting parameters, effectively reducing the number of independent parameters to three for lamellar microemulsions.

VI. MORPHOLOGY VISUALIZATION

The clipped random wave model also lends itself easily to computer rendering, allowing us to visualize the morphology of an oil-water interface defined by $\psi(\mathbf{r})=\alpha$. For ease of calculation, we first re-express Eq. (2) as a sum over wavevectors instead of individual cosine waves, resulting in

$$\psi(\mathbf{r})=\mathrm{Re}\sum_{\mathbf{k}}\left(\frac{2\pi}{L}\right)^{3/2}\sqrt{6f(\mathbf{k})}A(\mathbf{k})e^{i\mathbf{k}\cdot\mathbf{r}+i\phi(\mathbf{k})}, \tag{19}$$

where L is the length of the real-space lattice we want to generate and $A(\mathbf{k})$ is a random number uniformly distributed within the interval [0,1]. Here we have used the complex exponential representation of the cosine function, and each term is weighted by the aggregate wave vector distribution function $\sqrt{6f(\mathbf{k})}$. The additional factor $A(\mathbf{k})$ takes into account the possibility of destructive interference in Eq. (2) between cosine waves with the same wave vector but different phases.

$\psi(\mathbf{r})$ is thus readily calculated by performing an inverse discrete Fourier transform over a sufficiently large 3D lattice of $\mathbf{k}$ values, with each wavevector assigned a randomly generated $\phi(\mathbf{k})$ and $A(\mathbf{k})$. The resulting order parameter field can then be clipped at the appropriate level α to generate distinct oil-water domains.

The result of one such computation is shown on the next page, using the SDF from Eqs. (14) and (15). At first glance, the structure shown above is surprising because it does not resemble the conventional picture of extended lamellar planes. However, upon closer inspection, small domains can be seen where the internal structure is locally lamellar (white

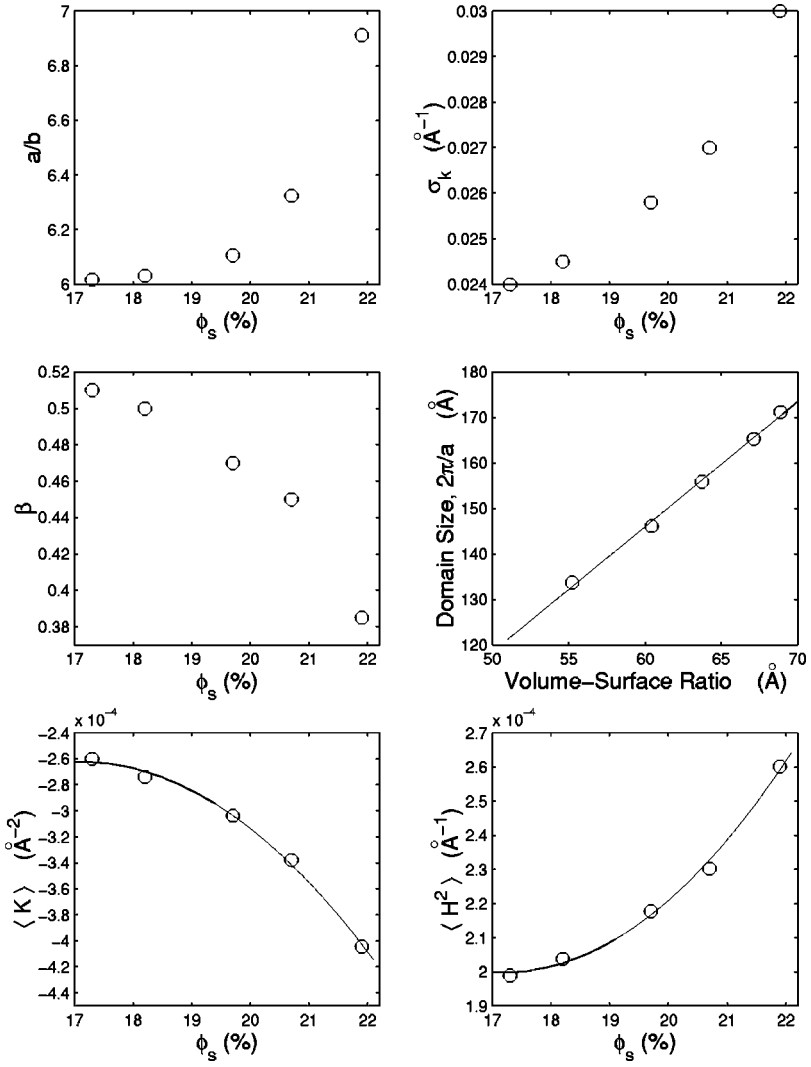

FIG. 4. Variation of parameters for lamellar samples.

lines), but the orientations of the lamellar sheets differ across domains. Also, there seems to be many ''holes'' in the lamellar planes.

This structure is actually consistent with the results from Figs. 4 and 5 which show that $\xi/d \approx 2$, thus the local order should only persist for about 2 or 3 domain lengths before decaying away. Furthermore, the highly negative mean Gaussian curvature indicates the proliferation of passages between lamellar sheets, which is readily observed in Fig. 6.

In addition to elucidating the real space structure of the microemulsion, this method also allows us to derive the probability distributions of the Gaussian and mean square curvatures, rather than merely knowing their average values from Fig. 4. Using Eq. (19), the spatial derivatives of $\psi(\mathbf{r})$ can be easily calculated. Since the microemulsion interface is represented by $\psi(\mathbf{r})=0$, we can make use of well-known equations in differential geometry to calculate the Gaussian and mean curvatures at each surface point [14]

$$K=\frac{1}{M^4}[\psi_{xx}\psi_{yy}\psi_z^2-\psi_{xy}^2\psi_z^2+2\psi_{xz}\psi_x(\psi_y\psi_{yz}-\psi_z\psi_{yy}) + (\text{permutations})] \tag{20}$$

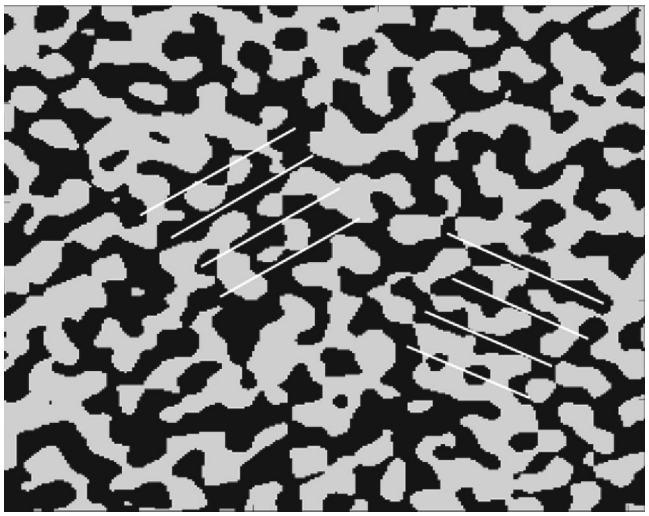

FIG. 5. 2D slice (size 2048×2048 Å) of a lamellar microemulsion in real space ($\varphi_s=21.9\%$). Small domains with a lamellarlike internal structure can be observed, some of which are marked with white lines.

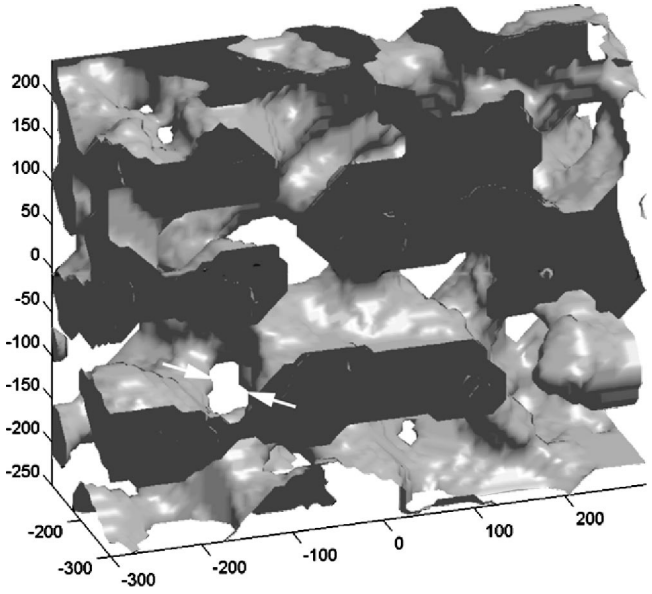

FIG. 6. Section of a lamellar microemulsion in real space ($\varphi_s = 21.9\%$). A passage defect (marked by arrows) can be clearly observed. The disordered nematic structure is the result of a proliferation of such defects. Length scales are marked in angstroms.

$$H = \frac{1}{2M^3}[\psi_{xx}(\psi_y^2+\psi_z^2) - 2\psi_x\psi_y\psi_{xy} + \text{permutations}],$$

where ''permutations'' indicates additional terms obtained by cyclic permutation, and where

$$M = \sqrt{\psi_x^2+\psi_y^2+\psi_z^2}. \tag{21}$$

Using this procedure, the probability distributions of K and H can thus be determined. As we can see from the result of one such calculation in Fig. 7, the distribution function $P(H)$ is symmetrically distributed around $H=0$, which is expected for an isometric microemulsion. On the other hand, the distribution function $P(K)$ is peaked and skewed towards the negative values, which is natural for an interface with a negative average Gaussian curvature. However, there is a small but significant probability that positive values of Gaussian curvature can be found at some points on the interface. This means that an arbitrary point of the interface may not always have a saddle-point configuration, but may instead have locally spherical curvatures.

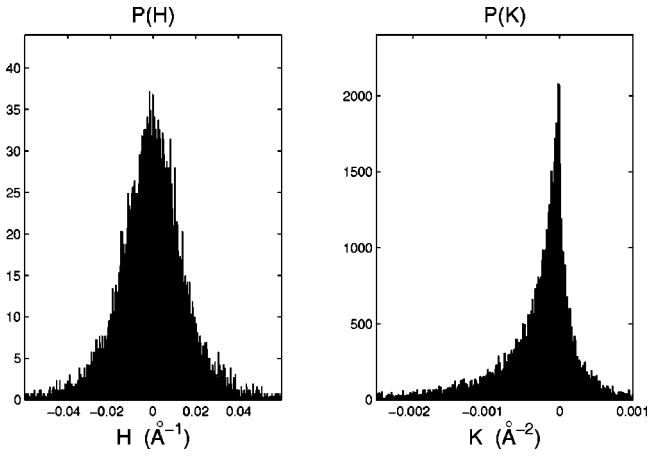

FIG. 7. Distribution of the mean curvature $P(H)$ (left) and Gaussian curvature $P(K)$ (right) for a $\varphi_s = 21.9\%$ sample. The values of $\langle K\rangle$ and $\langle H^2\rangle$ calculated from these distributions agree with the results given in Fig. (4) which were obtained from Eq. (7).

VII. CONCLUSION

We have made measurements of the scattering intensity of highly dilute lamellar microemulsions and analyzed the results using a spectral density function derived by maximization of generalized entropy. Indeed, the morphology of the lamellar structure we observe in Figs. 5 and 6 is surprising at first sight. However, the fact that this morphology is completely consistent with the scattering pattern observed leads us to conclude that in this type of dilute lamellar microemulsion the structure may in fact contain a large number of defects. These defects are due to the small bending constant of the surfactant film and vanishing interfacial tension of the oil-water interface which result in large thermal fluctuations. Since the intermembrane distance is too great, these fluctuations are not compensated by the usual Helfrich steric repulsion. Furthermore, our findings are in agreement with studies of lamellar systems near a sponge-lamellar transition using freeze-fracture electron microscopy [15], which show clearly the existence of membranes perforated by a large number of passage defects. It is thus reasonable to conclude that extended lamellar planes are actually not stable in this region of the phase diagram close to the boundary between the lamellar and disordered bicontinuous phases.

ACKNOWLEDGMENTS

We would like to thank the instrument scientists at SAND (IPNS), Dr. P. Thiyagarajan, Dr. D.G. Wozniak, and Dr. K.C. Littrell, for their help with the experiments. We would also like to thank Dr. S.M. Choi for invaluable discussions regarding the fitting of the clipped random wave model to the experimental data. This work was supported by a grant from the U.S. Department of Energy.

APPENDIX: DERIVATION OF ORDER PARAMETER EQUATION FOR MORPHOLOGY VISUALIZATION

To apply Fourier techniques when using the computer to generate the order parameter field, we first need to re-express Eq. (2) as a sum over the wave vectors $\mathbf{k}$ rather than as a sum over individual cosine waves. This is accomplished by performing the sum over cosine waves with the same $\mathbf{k}$ but different ϕ_n.

Using the complex exponential representation of the cosine, we can rewrite the order parameter equation as

$$\psi(\mathbf{r}) = \sqrt{\frac{1}{2N}}\sum_1^N e^{i\mathbf{k}_n\cdot\mathbf{r}+i\phi_n} + e^{-i\mathbf{k}_n\cdot\mathbf{r}-i\phi_n}$$

$$= \sqrt{\frac{1}{2N}}\sum_{\mathbf{k}}\sum_{\mathbf{k}_n=\mathbf{k}} e^{i\mathbf{k}_n\cdot\mathbf{r}+i\phi_n} + e^{-i\mathbf{k}_n\cdot\mathbf{r}-i\phi_n}. \tag{A1}$$

For the inner sum, the common factor $\exp(i\mathbf{k}_n\cdot\mathbf{r})$ can be factored out, leaving a sum of unit vectors on the complex plane

$$\sum_{\mathbf{k}_n=\mathbf{k}} e^{i\mathbf{k}_n\cdot\mathbf{r}+i\phi_n}=e^{i\mathbf{k}\cdot\mathbf{r}}(e^{i\phi_1}+e^{i\phi_2}+e^{i\phi_3}+\cdots). \quad \text{(A2)}$$

Since the phases ϕ_n are completely random, the superposition of these unit vectors results in a vector also with random magnitude and phase. The magnitude of this net vector, however, has a maximum value $p(\mathbf{k})$, given by the number of cosine waves with the same wave vector (in the case where all the phases ϕ_n are exactly equal). The sum can therefore be succinctly represented as

$$\sum_{\mathbf{k}_n=\mathbf{k}} e^{i\mathbf{k}_n\cdot\mathbf{r}+i\phi_n}=p(\mathbf{k})A(\mathbf{k})e^{i\mathbf{k}\cdot\mathbf{r}+i\phi(\mathbf{k})}, \quad \text{(A3)}$$

where $A(\mathbf{k})$ is a random number uniformly distributed in the interval $[0,1]$ and $\phi(\mathbf{k})$ also a random number in the range $[0,2\pi)$.

Substituting these results into Eq. (A1), we arrive at the equation

$$\psi(\mathbf{r})=\sum_{\mathbf{k}} p(\mathbf{k})A(\mathbf{k})(e^{i\mathbf{k}\cdot\mathbf{r}+i\phi(\mathbf{k})}+e^{-i\mathbf{k}\cdot\mathbf{r}-i\phi(\mathbf{k})}), \quad \text{(A4)}$$

where we have absorbed other normalization factors into $p(\mathbf{k})$. We then normalize Eq. (A4) by calculating

$$\begin{aligned}\langle|\psi|^2\rangle=&\sum_{\mathbf{k},\mathbf{k}'} p(\mathbf{k})p(\mathbf{k}')\langle A(\mathbf{k})A(\mathbf{k}')\rangle\\ &\times[e^{i(\mathbf{k}+\mathbf{k}')\cdot\mathbf{r}}\langle e^{i\phi(\mathbf{k})}e^{i\phi(\mathbf{k}')}\rangle\\ &+2e^{i(\mathbf{k}-\mathbf{k}')\cdot\mathbf{r}}\langle e^{i\phi(\mathbf{k})}e^{-i\phi(\mathbf{k}')}\rangle\\ &+e^{-i(\mathbf{k}+\mathbf{k}')\cdot\mathbf{r}}\langle e^{-i\phi(\mathbf{k})}e^{-i\phi(\mathbf{k}')}\rangle]. \quad \text{(A5)}\end{aligned}$$

Since $\langle e^{i\phi(\mathbf{k})}\rangle = 0$, therefore

$$\begin{aligned}\langle e^{i\phi(\mathbf{k})}e^{i\phi(\mathbf{k}')}\rangle&=0,\\ \langle e^{i\phi(\mathbf{k})}e^{-i\phi(\mathbf{k}')}\rangle&=\delta_{\mathbf{k},\mathbf{k}'}, \quad \text{(A6)}\\ \langle e^{-i\phi(\mathbf{k})}e^{-i\phi(\mathbf{k}')}\rangle&=0,\end{aligned}$$

which reduces Eq. (A5) to

$$\langle|\psi|^2\rangle=\sum_{\mathbf{k}} 2p^2(\mathbf{k})\langle A^2(\mathbf{k})\rangle. \quad \text{(A7)}$$

Also, $\langle A^2(\mathbf{k})\rangle=1/3$ since $A(\mathbf{k})$ is uniformly distributed between 0 and 1. Imposing the normalization constraint of $\langle|\psi|^2\rangle=1$, we now obtain

$$\sum_{\mathbf{k}} \frac{2}{3}p^2(\mathbf{k})=1. \quad \text{(A8)}$$

If this equation is compared to the normalization condition on $f(\mathbf{k})$ in Eq. (10), we can immediately see that

$$\sum_{\mathbf{k}} \frac{2}{3}p^2(\mathbf{k})=\int f(\mathbf{k})d^3\mathbf{k}, \quad \text{(A9)}$$

which results in the identity

$$p(\mathbf{k})=\left(\frac{2\pi}{L}\right)^{3/2}\sqrt{\frac{3f(\mathbf{k})}{2}}. \quad \text{(A10)}$$

Substitution of Eq. (A10) into Eq. (A4) yields

$$\begin{aligned}\psi(\mathbf{r})&=\sum_{\mathbf{k}}\left(\frac{2\pi}{L}\right)^{3/2}\sqrt{\frac{3f(\mathbf{k})}{2}}A(\mathbf{k})(e^{i\mathbf{k}\cdot\mathbf{r}+i\phi(\mathbf{k})}+e^{-i\mathbf{k}\cdot\mathbf{r}-i\phi(\mathbf{k})})\\ &=\mathrm{Re}\sum_{\mathbf{k}}\left(\frac{2\pi}{L}\right)^{3/2}\sqrt{6f(\mathbf{k})}A(\mathbf{k})e^{i\mathbf{k}\cdot\mathbf{r}+i\phi(\mathbf{k})}, \quad \text{(A11)}\end{aligned}$$

which was the equation used in the paper, Eq. (19).

The correctness of this expression can then be checked by calculating the two point correlation function $g(\mathbf{r})=\langle\psi(\mathbf{r})\psi(0)\rangle$,

$$\begin{aligned}g(\mathbf{r})=&\sum_{\mathbf{k},\mathbf{k}'}\left(\frac{2\pi}{L}\right)^3\frac{3}{2}\sqrt{f(\mathbf{k})f(\mathbf{k}')}\langle A(\mathbf{k})A(\mathbf{k}')\rangle\\ &\times[e^{i\mathbf{k}\cdot\mathbf{r}}\langle e^{i\phi(\mathbf{k})}e^{i\phi(\mathbf{k}')}\rangle+2e^{i\mathbf{k}\cdot\mathbf{r}}\langle e^{i\phi(\mathbf{k})}e^{-i\phi(\mathbf{k}')}\rangle\\ &+e^{-i\mathbf{k}\cdot\mathbf{r}}\langle e^{-i\phi(\mathbf{k})}e^{-i\phi(\mathbf{k}')}\rangle], \quad \text{(A12)}\end{aligned}$$

which, using the relations given in Eq. (A6), reduces to

$$g(\mathbf{r})=\sum_{\mathbf{k}}\left(\frac{2\pi}{L}\right)^3 3f(\mathbf{k})\langle A^2(\mathbf{k})\rangle e^{i\mathbf{k}\cdot\mathbf{r}}. \quad \text{(A13)}$$

Since $\langle A^2(\mathbf{k})\rangle = 1/3$, therefore we can see that $g(\mathbf{r})$ is just the Fourier transform of the spectral function $f(\mathbf{k})$,

$$g(\mathbf{r})=\sum_{\mathbf{k}}\left(\frac{2\pi}{L}\right)^3 f(\mathbf{k})e^{i\mathbf{k}\cdot\mathbf{r}}, \quad \text{(A14)}$$

which is equivalent to Eq. (4) for a continuous isotropic distribution of wave vectors.

[1] G. Porte, J. Phys.: Condens. Matter **4**, 8649 (1992).

[2] C.R. Safinya, D. Roux, G.S. Smith, S.K. Sinha, P. Dimon, N.A. Clark, and A.M. Bellocq, Phys. Rev. Lett. **57**, 1193 (1986).

[3] W. Helfrich, Z. Naturforsch. A **33**, 305 (1978).

[4] L. Golubović, Phys. Rev. E **50**, R2419 (1994).

[5] P. Pieruschka, Phys. Rev. E **52**, 3989 (1995).

[6] M. Teubner and R. Strey, J. Chem. Phys. **87**, 3195 (1987); S.H. Chen, S.L. Chang, and R. Strey, *ibid.* **93**, 1907 (1990).

[7] N.F. Berk, Phys. Rev. Lett. **58**, 2718 (1987).

[8] S.H. Chen, D.D. Lee, and S.L. Chang, J. Mol. Struct. **296**, 259 (1993); D.D. Lee and S.H. Chen, Phys. Rev. Lett. **73**, 106 (1994); S.H. Chen, D.D. Lee, K. Kimishima, H. Jinnai, and T. Hasimoto, Phys. Rev. E **54**, 6526 (1996); S.H. Chen and S.M.

Choi, J. Appl. Crystallogr. **30**, 755 (1997).
[9] P. Debye, H.R. Anderson, Jr., and H. Brumberger, J. Appl. Phys. **28**, 679 (1957).
[10] M. Teubner, Europhys. Lett. **14**, 403 (1991).
[11] C. Tsallis, J. Stat. Phys. **52**, 479 (1988); E.M.F. Curado and C. Tsallis, J. Phys. A **24**, L69 (1991).
[12] A.M.C. de Souza and C. Tsallis, Physica A **236**, 52 (1997).
[13] P. Thiyagarajan (private communication). We would like to thank Dr. P. Thiyagarajan of IPNS, Argonne National Laboraties, for supplying numerical values of the resolution function widths.
[14] S. Hyde, *The Language of Shape: The Role of Curvature in Condensed Matter—Physics, Chemistry and Biology* (Elsevier, Amsterdam, 1997).
[15] R. Strey *et al.*, Langmuir **6**, 1635 (1990).